IEEE Journal of Microwaves

Received 6 October 2021; revised 2 November 2021; accepted 8 November 2021. Date of publication 30 November 2021; date of current version 7 January 2022.

Digital Object Identifier 10.1109/JMW.2021.3126927

Screen-Printable Flexible Textile-Based Ultra-Broadband Millimeter-Wave DC-Blocking Transmission Lines Based on Microstrip-Embedded Printed Capacitors

MAHMOUD WAGIH (Member, IEEE), ABIODUN KOMOLAFE (Member, IEEE), AND NICHOLAS HILLIER

(Regular Paper)

School of Electronics and Computer Science, University of Southampton, SO171BJ Southampton, U.K.

CORRESPONDING AUTHOR: M. Wagih (e-mail: mahm1m19@soton.ac.uk).

This work was supported in part by the U.K. Engineering and Physical Sciences Research Council (EPSRC) under Grant EP/P010164/1, and in part by the European Commission through the EnABLES Project under Grant 730957.

This article has supplementary downloadable material available at https://doi.org/10.1109/JMW.2021.3126927, provided by the authors.

ABSTRACT In this paper, a novel multi-layered microstrip line with built-in parallel-plate capacitors is proposed for DC-blocking applications, with its transmission characteristics measured up to 50 GHz. The microstrip lines are fabricated via screen printing directly onto polyurethane films laminated on standard textile substrates which would otherwise be unsuitable for printing. Compared to a standard microstrip line on the same substrate, the proposed 10 cm-long line on felt (with an embedded 44 pF capacitance) suffers from less than 0.1 dB higher insertion loss up to 4 GHz. Furthermore, varying the overlapping length of the lines and hence the capacitance enables the realization of DC blocking and −3 dB high-pass filtering with pass-bands starting between 88 MHz and 1.2 GHz. This is achieved without altering the cut-off frequency of the microstrip line's mode-free propagation, measured up to 50 GHz, exhibiting a low attenuation of 0.32 dB/mm at 50 GHz on a felt fabric substrate. Compared to a lumped capacitor, the proposed microstrip-embedded printed capacitor demonstrates a significant improvement in mechanical reliability, withstanding over 10,000 bending cycles, and RF power handling with under 6 °C temperature rise at 1 W. The lines are fabricated on two textile substrates and their transmission characteristics were measured up to 50 GHz, which represents the highest frequency characterization of textile-based lines to date, demonstrating a stable group delay and insertion losses. Based on the proposed multi-layered integration method, low-cost screen-printed microstrip-embedded capacitors on textiles can be used for microwave applications up to mmWave bands.

INDEX TERMS Additive manufacturing, capacitors, DC block, high-pass filter, microstrip lines, printed capacitors, radio frequency (RF), textile capacitors, transmission lines.

I. INTRODUCTION

Flexible, printable, and conformable microwave and millimeter-wave (mmWave) components have attracted significant research interest for a variety of Internet of Things (IoT) and 5G+/6G applications [1], [2]. Wireless communication antennas [3], energy harvesting rectennas [4], mmWave imaging arrays [5], and RFIC packaging [6] are among the applications tackled through additive manufacturing of microwave and mmWave distributed components. Furthermore, the realization of individual components such as RF capacitors using inkjet [7] and 3D printing [8] has been demonstrated. In low-cost, large-area, printed electronics, and wearable applications, it is desirable to minimize the lumped components count in the system and utilize printed components to maximize flexibility [9].

Shortly after the early development of planar microstrip transmission lines, DC-blocking microstrip lines attracted significant interest [10]–[12], [12], [13]. In planar microstrip technology, DC-blocks are typically realized using coupled lines [13]. As a result, they are often integrated within filters

or impedance transformers [14], and have a narrow pass-band. "Broadband" DC-blocking lines have then been reported based on a variety of planar interdigital capacitors and tightly-coupled lines [13], integrated within a signal line [11] or a microstrip ground plane [12]. Yet, their bandwidth rarely exceeds 100% relative bandwidth making them less effective than lumped capacitors for ultra-broadband DC blocking applications, where the pass-band is limited to a single-band such as the Ka-band [12] or the V-band [15]. In addition, the use of interdigital capacitors requires a high resolution fabrication method, not achievable using standard PCB manufacturing, should the transmission line achieve a sufficiently high capacitance for a sub-1 GHz pass-band [16]. Emerging discrete capacitors have been shown operating up to 16 GHz using artificially engineered materials realized using additive manufacturing [8]. However, the achieved high (>1 pF) capacitance is still dependent on a discrete, rigid, lumped component, which is undesirable in flexible and wearable applications. Furthermore, despite the growing popularity of additively-manufactured microwave components including multi-layered microstrip lines operating up to 10 GHz [17], there are no reported broadband DC-blocking lines implemented using additive manufacturing on low-cost flexible substrates. To explain, while paper-based capacitively-coupled coplanar waveguides were realized for 1-5GHz applications, their measured S_{21} response was highly unstable with an insertion loss over 2 dB/cm, as low as 5GHz, with a non-uniform phase response [18].

Following the increased popularity of additively manufactured RF components, printed capacitors have been realized on flexible polymer [7], [19], and silicon substrates [20]. Inkjet printing, owing to its ability to produce thin dielctric layers was used to realize RF capacitors on Liquid Crystal Polymer (LCP) with a sub-3 GHz cut-off-frequency [7]. Nevertheless, the demonstration of microwave inkjet printed capacitor, up to 3 GHz, has been limited to smooth and homogeneous substrates such as LCP and silicon, using a layer of costly SU-8 polymer as the bonding interface. A range on inkjet printed microwave and mmWave transmission lines have also been demonstrated and characterized up to 30 GHz, on smooth low-loss LCP substrates [3]. Although a screen-printed textile-based mmWave antenna was recently demonstrated at 77 GHz [5], all reported textile-based transmission measurements of textile-based printed transmission lines were limited to sub-10 GHz measurements [21]. To illustrate, while several aerosol-jetted lines were characterized up to 110 GHz [22], [23], such implementations are only possible on smooth and homogeneous substrates with high thermal reliability, such as LCP and polyimide, and are not suitable for use with rough substrates such as conventional fabrics and paper. In addition, the mechanical reliability of such implementations against repeated bending, typical for wearables, was not explored.

On textiles and other rough lossy substrates, realizing high-frequency components resembles a challenge. Printed interface layers as well as laminated polymers have been used to enable sub-6 GHz antennas to be implemented on fabrics [24], [25]. At mmWave bands, antennas and rectennas with distributed matching have been realized on textile substrates using homogeneous copper films and laminates [26], [27], and more recently using screen printing to realize a simple microstrip antenna array [5]. Active microwave circuits have also been integrated in embroidered e-textiles but only in the sub-6 GHz spectrum [28]. Lumped textile components, namely capacitors, have been realized using inkjet printing but only for low frequency applications [29], where all the sub-6 GHz RF passives have only been demonstrated on smooth polymers and up to 5GHz [19].

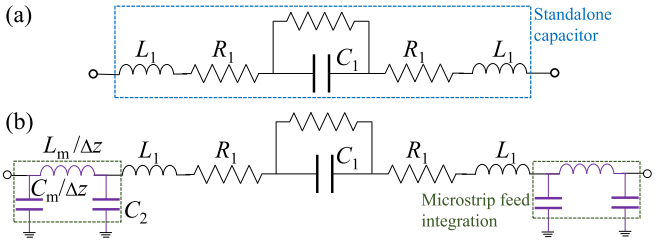

FIGURE 1. Equivalent circuit models: (a) the standalone printed capacitor; (b) the microstrip-integrated capacitor, including a loss-less transmission line equivalent circuit per unit length ($/\Delta z$).

In this paper, a novel multi-layered microstrip line is proposed for ultra-broadband DC-blocking applications. The lines are implemented on a textile substrate with impregnated capacitors based on a standard low-resolution screen printing method. Operating up to 50 GHz, the proposed DC-blocking microstrip line represents the highest frequency application to date of a printed capacitor, and the widest bandwidth DC-block reported in literature. Moreover, the presented 50 GHz transmission characteristics represent the highest frequency characterization of a printed ink-based microstrip implemented on a textile substrate. In Section II, the design and fabrication method of the proposed line are presented. Section III then presents the simulated and measured performance of the microstrip lines compared to conventional lumped capacitors. Section IV presents the modelled and measured transmission results of the capacitor-impregnated lines up to 50 GHz, demonstrating their suitability for mmWave applications.

II. PRINTABLE EMBEDDED MICROSTRIP CAPACITORS

A. MICROSTRIP CAPACITOR DESIGN AND SIMULATION

The proposed capacitor structure is based on a multi-layered microstrip line, with a low-cost dielectric laminate embedded between the overlapping lines. The equivalent circuit model of a typical lumped capacitor is shown in Fig. 1(a). The capacitance of the overlap region, C_1, can be calculated using the simple parallel-plate capacitor formula given by

$$C_1 = \epsilon_0 \epsilon_r \frac{A}{t}, \tag{1}$$

where A is the area of the overlap between both lines ($x \times w$), and t is the height of the dielectric layer embedded between both microstrip sections. Fig. 2 shows the layout (a) and

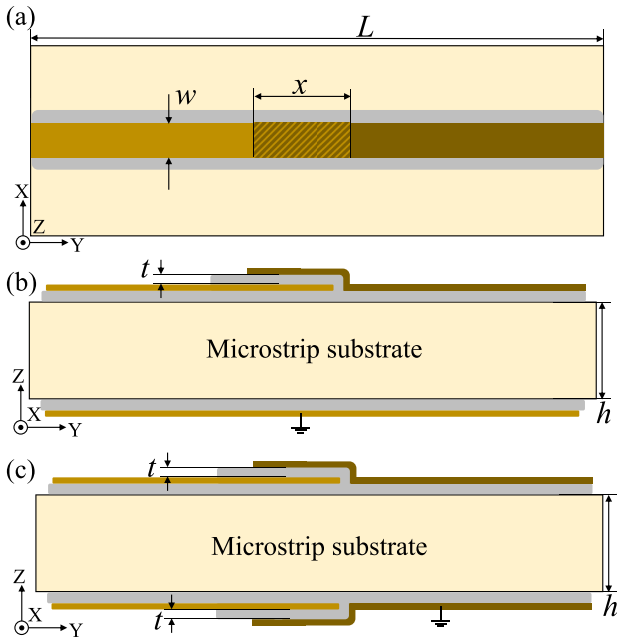

FIGURE 2. Layout of the proposed microstrip-embedded capacitor: (a) XY layout of the microstrip line. (b) cross-section of a DC-blocking line. (c) cross-section of a DC blocking line and ground.

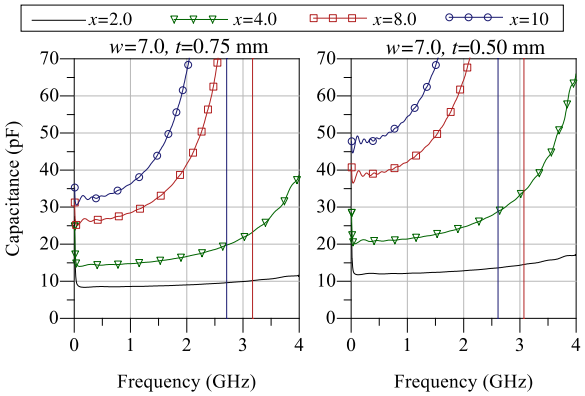

FIGURE 3. Simulated capacitance of the standalone capacitors, with no microstrip feed, for two dielectric heights *t*.

cross-section (b) of the proposed microstrip-embedded capacitor. The analytical model is used to calculate the lines' response up to 50 GHz in Section IV-A, and its limitations are further discussed compared to the experimental characterization and full-wave simulations.

Prior to analyzing the performance of the microstrip-embedded capacitors, the standalone parallel-plate capacitors were simulated in CST Microwave Studio to verify the areal capacitance and observe the self-resonance frequency (SRF). The capacitors were simulated using a discrete port through the gap. A fixed line/capacitor width w is assumed with varying capacitor length x and dielectric height t. Fig. 3 shows the simulated capacitance of parallel plate capacitors for varying

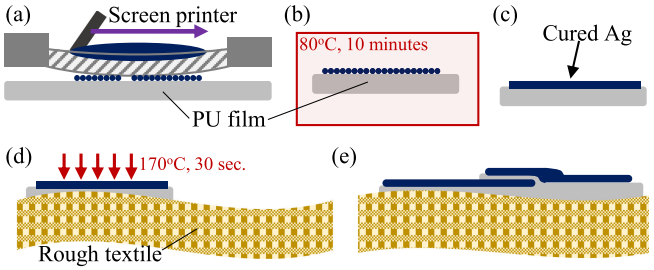

FIGURE 4. Fabrication steps of the proposed multi-layered screen-printed microstrip: (a) screen printing of the silver traces on the PU film. (b) silver traces curing. (c) the cured silver-on-PU trace ready for lamination onto other substrates. (d) heat-pressing on a rough textile substrate. (e) the assembled multi-layered structure using steps (a)-(d).

x and t. The capacitance has been calculated as

$$C = -1/(j\omega\Im\{Z_{11}\}), \tag{2}$$

where Z is the simulated input impedance calculated from the S_{11} of the standalone capacitor. Calculating the capacaitance from the measured or simulated Z_{11} introduces a non-physical frequency-dependent response near the SRF of the capacitors, where $\Im\{Z\}$ approaches 0. Therefore, the capacitance calculated from (2) is only valid below the SRF, in the "flat" region of the capacitance curve in Fig. 3. In the fabricated prototype, t will be limited by the fabrication process, and the interface layer used as the substrate in the microstrip transition.

As observed in Fig. 3, for a 75 μm-thick interface with $\epsilon_r = 3.2$, a capacitance over 10 pF could be achieved with a SRF >2 GHz. These t and ϵ_r values can be realized based on commercially-available polyimide (Kapton) or polyurethane films. The simulated capacitance and SRF are in line with previously reported RF capacitors realized using inkjet printed dielectrics of t <10 μm [20]. A reduction in t improves the areal capacitance and the SRF of a capacitor of the same value, as observed in Fig. 3.

B. TEXTILE-BASED MICROSTRIP CAPACITOR FABRICATION METHOD

The proposed microstrip line is demonstrated for wearable e-textile applications through screen printed silver traces on two textile substrates, 1.0 mm-thick felt and 0.44 mm-thick polyester cotton. Felt is a very rough non-woven fabric which is typically considered unsuitable for screen printing [30]. To overcome fabric roughness, a printed interface layer is typically used prior to depositing the conductive ink [24]. However, for a rough substrate such as felt, this will require several prints to achieve a smooth surface, increasing the fabrication time. Moreover, printed interface layers suffer from a high tanδ over 0.05 [30], making them a less-preferred choice for microwave applications.

Commercially-available polyurethane (PU) films, of 50 μm thickness, are used as the interface layer. First, the microstrip line is screen printed on the PU film, using low-temperature silver ink from Smart Fabric Ltd., as shown in Fig. 4. The printed films are cured at 70 °C before adhesion with the

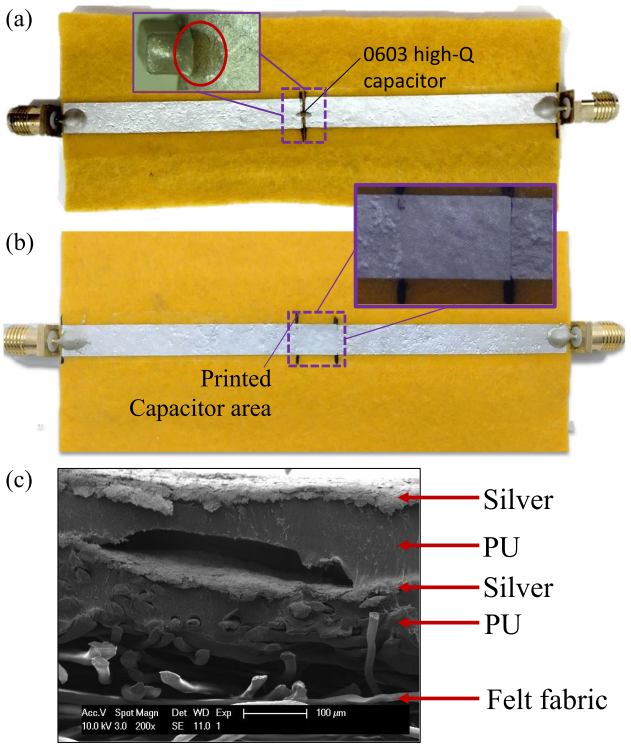

FIGURE 5. Photographs and micrographs of the fabricated capacitor on a felt substrate: (a) reference microstrip line with a lumped capacitor attached using conductive epoxy, with the inset showing the capacitor's failure after 10,000 bending cycles. (b) the proposed line with microstrip-embedded capacitance, the inset shows the line after 10,000 bending cycles. (c) SEM cross-section of the line's top layer and substrate showing its composition.

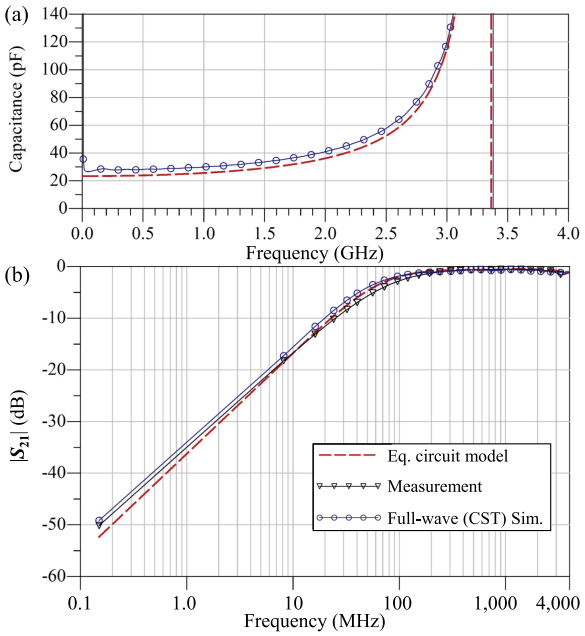

FIGURE 6. Performance of the 10 mm-long capacitor-impregnated microstrip: (a) analytical and full-wave numerical capacitance of the standalone capacitor. (b) analytical, numerical, and experimental S_{21} of the 10 cm-long microstrip line on felt with a 10 mm capacitor.

fabric substrate. The cured PU+silver films are then heat-pressed onto the felt for 30 s, at 170 °C. To realize the overlap and subsequently the capacitor, the silver microstrip line is bonded over the existing line, on the felt substrate, realizing the multi-layered structure shown in Fig. 4(e). For the UHF measurements, the SMA connectors are attached to the lines using silver-loaded conductive epoxy. As for the mmWave measurements, solder-free 2.4 mm connectors are used. The same approach could be utilized when assembling the ground plane, realizing a ground-embedded capacitor for DC blocks, as shown in Fig. 2(c). The fabricated prototypes are shown in Fig. 5.

The proposed fabrication method is chosen over inkjet printing due to its suitability for roll-to-roll manufacturing, and for achieving thicker conductor layers with rapid ink deposits (under 10 s) compared to the more time-consuming inkjet printing. Furthermore, the selected PU interface enables the realization of capacitors on a rough substrate, which was not used in any microwave application above 6 GHz, due to the difficulty of fabricating reliable fine-featured mmWave structures. As shown in the Scanning Electron Microscope (SEM) micrograph in Fig. 5(c), the PU film, relatively smooth comapred to the fabric, acts as an interface layer between the silver layers, enabling a more uniform structure than inkjet printed capacitors on textile susbtrates [29]. Methods including the use of wooden stencils have been proposed for standardizing the alignment of multi-layered textile-based lines and antennas [31], showing that the proposed approach can be applied in large-scale manufacturing.

III. CAPACITOR-IMPREGNATED MICROSTRIP CHARACTERIZATION

A. MICROSTRIP S-PARAMETERS MEASUREMENTS

The fabricated microstrip capacitor prototypes were measured using a Vector Network Analyzer (VNA) to characterize their two-port characteristics. A 3.5 mm TOSM calibration was used with a Rohde & Schwarz ZVB4 VNA, for the 150 KHz to 4 GHz measurements. Beyond 4 GHz, an Agilent E8361 A PNA, calibrated using a 1.85 mm SOLT E-calibration kit, was used to perform the s-parameter measurements up to 50 GHz. As the PNA measurements are limited by their lower sweep frequency of 10 MHz, essential to characterize the DC-blocking properties of the line, the low-frequency performance of the lines was fully characterized using the 150 kHz–4 GHz ZVB4 VNA.

In Fig. 6(a), the analytically calculated capacitance, calculated from the input impedance, is shown alongside the 3D simulated of a $w = 6$ mm and $x = 10$ mm standalone capacitor on felt, showing a close agreement. The line in which the capacitor was embedded, with $L = 100$ m, was fabricated and its S_{21} was measured experimentally. The measured forward transmission of a microstrip line fabricated with a 10 mm overlap is shown in Fig. 6(b). Alongside the measured s-parameters is the response of the equivalent capacitor circuit

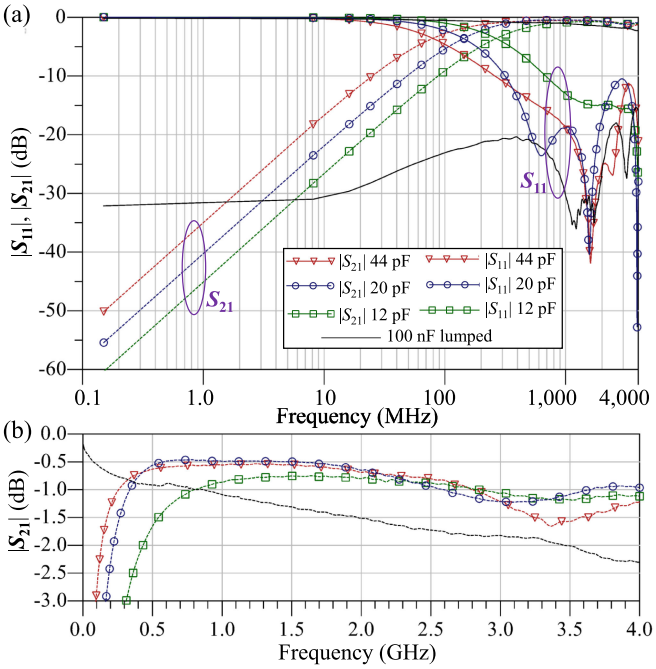

FIGURE 7. Measured s-parameters of the capacitor-impregnated microstrip lines showing over 60 dB S_{21} isolation at 150 kHz: (a) broadband $|S_{21,11}|$ logarithmic plot. (b) the pass-band of the lines; the 12-44 pF capacitances refer to the low-frequency parallel-plate printed capacitors.

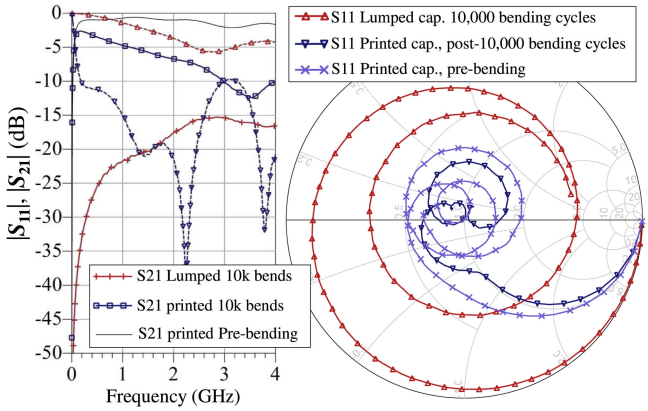

FIGURE 8. Measured s-parameters of the printed and lumped capacitor before and after 10,000 bending cycles showing the lumped capacitor's failure manifesting as a mismatched S_{11}.

model integrated with a closed-form microstrip model, as well as the CST full-wave model of the full line with the capacitive overlap. The equivalent circuit model parasitic parameters (i.e. inductance and resistance), from Fig. 6(a), were extracted from the simulated S_{11} of the standalone capacitor as $L_1 = 0.048$ nH, $R_1 = 0.1\ \Omega$. C_1 was calculated as 23.4 pF using (1) for $\epsilon_r = 2.2$, $x = 10$ mm, $w = 6$ mm, and $t = 0.05$ mm. Observing the simulated, calculated, and measured response, it can be observed that the lines are in good agreement with under 2 dB discrepancy below 1 MHz, and around 0.5 dB variation at higher frequencies.

Three lines have been fabricated with an overlap of 4, 8, and 10 mm overlap. $L = 100$ mm and $W = 6$ mm are chosen to maintain $Z_0 \approx 50\,\Omega$, based on the dielectric properties ($\epsilon_r = 1.2$; $\tan\delta = 0.02$) and $h = 1.1$. The lines had a measured low-frequency capacitance of 12, 20, and 44 pF, respectively. The difference between the measured capacitance and the ideal parallel-plate calculation using (1) is attributed to the non-uniform height of the dielectric layer. Furthermore, as observed in the SEM cross-section in Fig. 5(c), the capacitor PU dielectric interface suffers from non-uniformities manifesting as air gaps, which are expected to reduce the areal capacitance. The two-port s-parameters of the lines were measured using the VNA from 150 KHz to 4 GHz, Fig. 7 shows the measured s-parameters of the lines.

Observing Fig. 7(a), it can be observed that the capacitors provide over 50 dB high-pass filtering under 200 kHz. The pass-band, i.e. $S_{21} > -3$ dB, is found to have a tunable starting frequency ranging from 88 to 1.2 GHz, with the S_{21} response at higher frequencies being similar to a standard microstrip line with no capacitors or DC blocking elements. To explain, in the 1-4 GHz region, shown in Fig. 7(b), the lines maintain a stable S_{21} response indicating mode-free propagation along the microstrip line, as well as indicating that the cut-off frequency of the microstrip-embedded capacitor is higher than the operation frequency. For benchmarking, a standard microstrip line containing no DC-blocking capacitive overlap was measured experimentally. It was found that, up to 4 GHz, the S_{21} of the standard line was only 0.2 dB higher than the capacitor-impregnated line, highlighting that the capacitors add minimal losses to the lines.

B. MECHANICAL RELIABILITY

A further benefit of the proposed microstrip-embedded capacitor over lumped components is the improved mechanical reliability. To demonstrate the suitability of the rectifier to wearable applications, both the 0603 SMD capacitor and the proposed printed capacitor have been subjected to repetitive bending around a 5 mm radius for 10,000 cycles. The s-parameters of the lines were measured before and after bending, and are shown in Fig. 8.

As observed in the measured S_{21} in Fig. 8, the DC-blocking line based on the lumped capacitor fails after approximately 8,000 cycles by peeling off the silver traces. This is visually shown in the inset of Fig. 5(a), where not only does the capacitor detach from the microstrip line, but it also causes additional cracks around its original mounting pads. On the other hand, the proposed printed line maintains its functionality with a matched input impedance for over 10,000 bending cycles, resulting in an almost pristine appearance in the inset of Fig. 2(b). The increase in the insertion losses observed between the unbent and the bent lines, of approximately 8 dB, is attributed to the increase in the Ohmic resistance of the line, due to the micro-cracks in the printed silver traces. In addition, the repeated abrasion of the ground plane with the bending

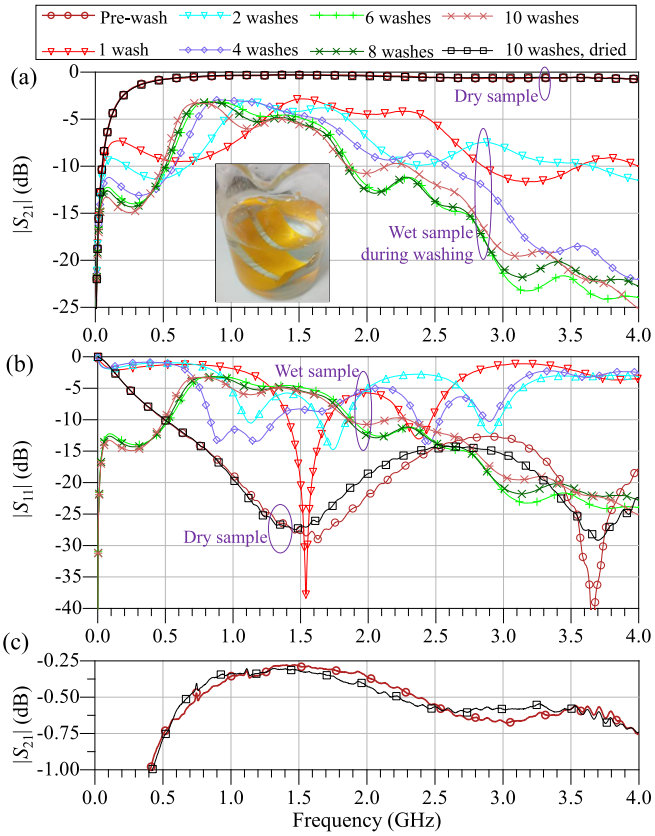

FIGURE. 9 **Measured s-parameters of the printed microstrip line with x = 5 mm (20 pF) capacitor for 10 washing cycles: (a) S_{21} before, during (wet), and after (dried) washing. (b) S_{11} before, during (wet), and after (dried) washing. (c) the pass-band of the lines showing minimal attenuation variation.**

rig over the 10,000 cycles increases the resistance across the ground plane, contributing to the additional losses. However, it can be seen through the input impedance plot, the $|S_{11}|$, as well as the $|S_{21}|$ that the microstrip line is still operational with a matched input impedance. This test represents a significant improvement in the number of bending cycles over existing reliability tests of RF textile components [32], which are often limited to under 500 bending cycles.

Along with being able to withstand repeated bending, flexible and wearable components are expected to withstand washing. The microstrip line with an embedded 5 mm-long capacitor has been subjected to 10 hand-washing cycles at room temperature. The line was washed for at least five minutes with continuous stirring for each cycle, before being dried out for a further 5 minutes prior to measurements. Hand washing has previously been used to investigate the performance of wearable mmWave antennas [27]. The s-parameters of the line have been measured before washing and after each washing cycle, and are shown in Fig. 9 . The washing test is detailed in the Supplementary Table 1.

Observing the measured S_{21} of the fully-dried sample after the 10 cycles, the change in the insertion losses is very minimal, demonstrating the printed silver traces' durability against water. Moreover, the matched $S_{11} < -10$ dB and the uniform S_{21} responses indicate that the lines maintain their functionality following repeated washing. The wet lines, where their mass increased by 100% due to the water content, suffer from a mismatched response as well as higher attenuation. This is attributed to the high real and imaginary permittivity of the water-soaked fabric, resulting in the line's impedance drifting away from 50 Ω. Such a change has been widely reported in flexible and e-textile components and has potential applications in humidity and moisture sensing [33], and will be present in any non-waterproof e-textile microwave component. The S_{21} at 150 kHz is under −50 dB for all measurements, with the fully-dried sample maintaining an $S_{21} = -56.5$ dB. Additional durability against machine washing and repeated abrasion can be achieved using an encapsulating superstrate based on a thin polyimide or PU film, which were previously used to enable flexible RFID antennas to withstand at least 30 machine washing cycles [34].

C. HIGH-POWER HANDLING

In addition to the improved mechanical reliability relative to a surface-mount 0603 RF capacitor, the distributed microstrip-embedded capacitor exhibits improved power handling compared to lumped parts. For example, commercially-available AVX 0603 SMD capacitors exhibit a power handling under 0.2 W, with the highest power handling capacitors (1210 package) rated at 0.34 W [35]. The power handling was defined in such measurements as the power level at which the capacitor's temperature rise exceeds 20 °C above room temperature [35].

In order to demonstrate the suitability of the capacitor-impregnated microstrip lines for high-power applications, the lines were tested for a >1 W RF input. A 41 dB gain Mini-Circuits ZHL-424W+ power amplifier (PA) was used to amplify the continuous wave (CW) input to the microstrip line, generated using the ZVB4 VNA at 2 GHz, using the setup shown in Fig 10(a) and (b). With a −5 dBm input at the amplifier (15 dBm CW input − 20 dB attenuator), the amplifier is expected to operate near its third-intercept with an output in excess of 30 dBm (1 W). The output of the amplifier was connected directly to the input of the felt-based line using an SMA adapter. The output of the line is connected to a 3 dB attenuator and subsequently fed into a 50 Ω SMA coaxial termination. The S_{11} of the resistor and attenuator-terminated line was measured to be under −20 dB. A Fluke Ti 125 thermal imager was used to measure the temperature across the line, shown in Fig. 10(c) and (d).

To begin with, a small-signal 2 GHz input (under 0 dBm) is fed through the line, to observe the temperature across the line under low-power signal transmission, and to observe the rise in temperature ΔT at high power levels. Fig. 10(c) shows the temperature across the line, 24 °C at the capacitive junction, prior to increasing the RF input power. The CW input was then raised to 15 dBm, resulting in over 1 W being transmitted through the microstrip line. Fig. 10(d) shows the thermal image of the microstrip line with a 1 W 2 GHz input.

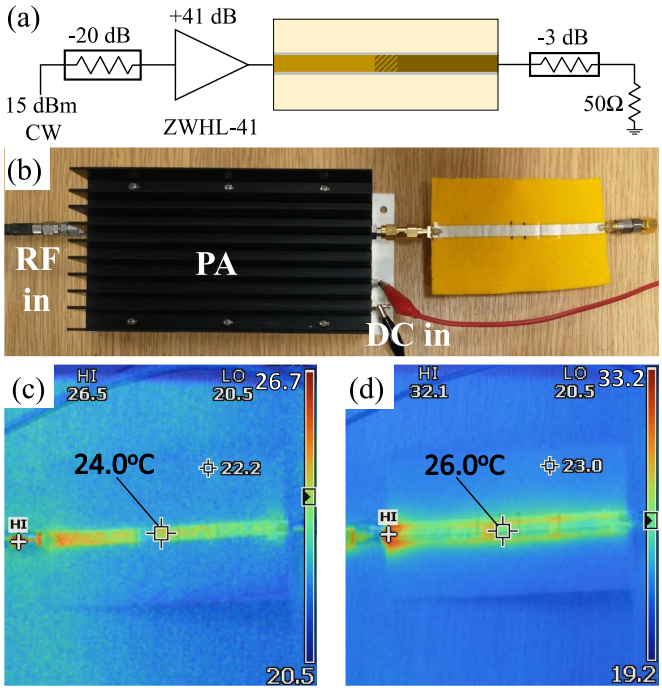

FIGURE 10. Demonstration of the microstrip capacitor's high power handling capabiilty: (a) experimental setup schematic. (b) setup photograph. (c) thermal image for a 2 GHz sub-0 dBm input. (d) thermal image for a 2 GHz 1 W input.

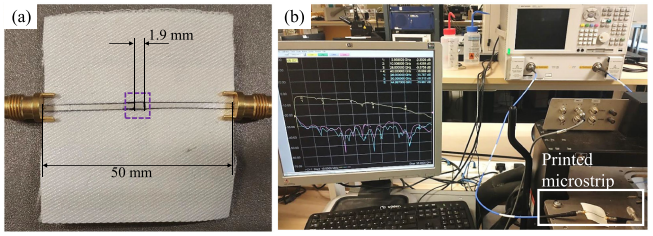

FIGURE 11. Photographs of (a) the polyester-cotton microstrip-embedded capacitor with the 2.4 mm coaxial connectors. (b) the measurement setup.

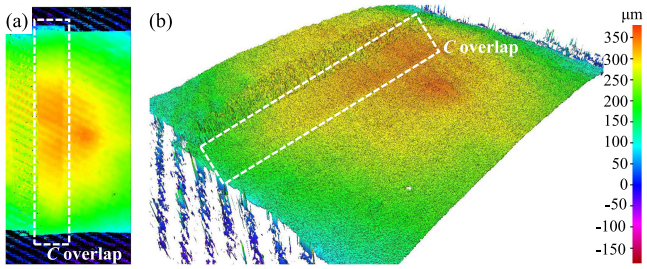

FIGURE 12. Measured surface profile of the DC blocking line on a woven polyester-cotton substrate: (a) 2D plot of the height at the signal-line capacitor. (b) 3D plot of the ground plane capacitor.

Based on the observed 2 °C rise for a 1 W input, it can be observed that the power handling of the microstrip line is over 1 W, significantly higher than that of the commercial capacitors which undergo a 20 °C temperature rise for a <0.4 W input. Moreover, throughout the entire line, it can be observed that the maximum ΔT is under 6 °C, indicating the line's suitability for high-power applications such as a PA's output bias network. The measured thermal response is linked to the measured low insertion loss, in Fig. 7(b), of 0.5 dB, indicating that around 100 mW from the 1 W 2 GHz signal dissipates through the line. On the other hand, the lumped capacitor line had an S_{21} of −1.5 dB at 2 GHz, explaining the higher ΔT of lumped capacitors, [35], compared to the printed microstrip-embedded capacitor.

IV. MILLIMETER-WAVE DC-BLOCKING MICROSTRIP LINE

A. MMWAVE CAPACITOR-IMPREGNATED MICROSTRIP DESIGN AND CHARACTERIZATION

The proposed DC blocking lines were investigated for operation in the mmWave spectrum. An additional capacitor is realized based on 0.44 mm-thick woven polyester cotton fabric. The dielectric properties of the substrate were measured using a T-resonator to be $\epsilon_r = 1.7$ and $\tan\delta = 0.017$ at 4 GHz. The lines were designed with $L = 50$ mm and $w = 1.6$ mm, to maintain $Z_0 \approx 50\ \Omega$. This is attributed to the overall substrate height increase to 0.53 mm after laminating the PU films onto the fabric. Fig. 11 shows photographs of the connectorized capacitor-impregnated microstrip and the experimental setup. The line was assembled with a capacitive DC-blocking element of $x = 1.9$ mm embedded within the signal trace (top-layer) and the ground plane (bottom-layer), not visible in the photograph.

The height and length of the capacitive overlap, as well as the surface roughness of the silver trace were measured using an Alicona optical surface profiler. Fig. 12 shows the measured 3D surface profile of the microstrip line. It is observed in Fig. 12(a) that the height of the microstrip line h can vary by over 200 μm, explaining the observed Z_0 non-uniformities hindering an $S_{11} < -20$ dB. Moreover, the height of the printed microstrip traces closely follows the diagonal weave pattern of the substrate, causing height variations up to 50 μm. While the uncoated fabric's measured roughness exceeded 100 μm, the surface roughness of the printed silver line varied in the 5–40 μm range. An RMS roughness of 25 μm was subsequently introduced to the 3D CST full-wave simulations of the line based on the loss model from [36].

The polyester-cotton microstrip line, in Fig. 11(a), was simulated with the 2.4 mm connectors. The simulated E-field over the line, excited using a wave-port, are shown in Fig. 13, from 10 MHz to 50 GHz (the measurement bandwidth). The DC-blocking and high-pass filtering properties of the line are clearly visualized in Fig. 13(a) and (e), where under −60 dB of the maximum E-field propagates to the output. At 4, 25, and 50 GHz, it can be observed that the signals transition smoothly across the gap. However, the 50 GHz E-field plot shows the radiative losses of the microstrip line which would be present in a microstrip line with the same dimensions,

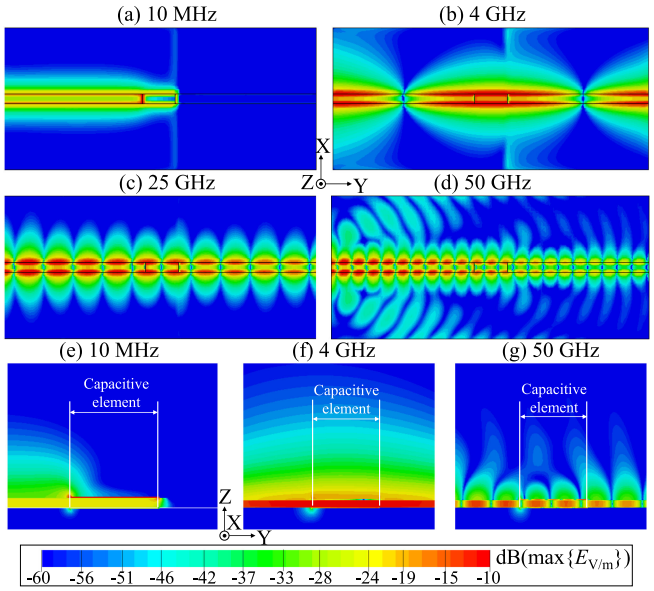

FIGURE 13. Simulated *E*-field plots of the microstrip line: (a) XY fields at 10 MHz showing the low-*f* stopping properties. (b) 4 GHz XY plot. (c) 25GHz XY plot. (d) 40 GHz XY plot. (e) cross-sectional YZ plot of the capacitor at 10 MHz. (f) YZ plot at 4 GHz. (g) YZ plot at 50 GHz.

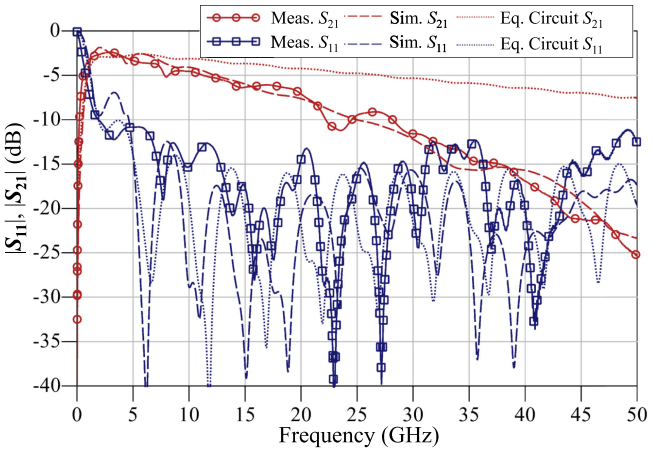

FIGURE 14. Simulated (dashed), analytically-calculated (dotted), and measured (solid) s-parameters of the polyester-cotton microstrip line, demonstrating its functionality up to 50 GHz.

regardless of the existence of the DC-blocking capacitor. Furthermore, despite there being a ground-plane slit at the ground DC blocking capacitor, it can be observed that no radiative *E*-field losses are caused by the gap, as shown in the cross-sections in Fig. 13(f) and (g). The simulated s-parameters response of the microstrip line, shown in the supplementary Fig. 3, without coaxial connectors, indicates its ability to operate up to 110 GHz with a matched S_{11} response, subject to the materials maintaining their properties in the 50–110 GHz range. Nevertheless, our experimental validation is limited to 50 GHz due to the experimental setup, hence all the results presented in this section are limited to 50 GHz.

Fig. 14 shows the full-wave simulated, analytically-calculated using the equivalent circuit model in Fig. 1(b), detailed in the supplementary Fig. 2, and measured s-parameters of the line up to 50 GHz. The simulated and measured values exhibit a good agreement in the pass-band and attenuation up to 40 GHz. Beyond 40 GHz, it can be observed that the simulated losses are lower than the measured losses by around 2 dB, which is attributed to the inhomogeneity of the printed ink layer. Previously reported characterizations of printed lines in the mmWave range also exhibited discrepancies of over 5 dB beyond 30 GHz [23]. The conductivity of the silver layers in the CST model is $\sigma = 1\times10^5$ S/m with a surface roughness of 25 μm.

On the other hand, the closed-form microstrip model significantly underestimates the insertion losses increase with frequency from around 8 GHz. The lines were modelled based on the Hemispherical roughness model [37], implemented within Keysight ADS, with the measured roughness parameters shown in the Supplementary Fig. 2. This discrepancy highlights that a more accurate model aimed towards rough printed conductors may be required for accurate loss calculations, to match the level of accuracy achieved using the 3D full-wave simulated losses up to 40 GHz. However, as the circuit model in Fig. 1 is aimed towards the capacitor as opposed to the microstrip feed, improving the accuracy of the closed-form loss model is beyond the scope of this work. To illustrate, the close-agreement between the calculated, simulated, and measured S_{11} validates the proposed capacitor equivalent circuit model up to 50 GHz. A finer and more distributed model utilizing additional inductive L_1 and capacitve C_2 elements may be required to model the DC blocking line at frequencies beyond 50 GHz.

B. 50 GHZ PRINTED TEXTILE MICROSTRIP TRANSMISSION MEASUREMENTS

To-date, there has been limited investigations of the transmission properties of textile-based microstrip lines beyond 10 GHz. Embroidered lines were compared in [21] but only up to 6 GHz. Where mmWave antennas were implemented on textiles [27], [38], the insertion losses in fabric-based microstrip lines were experimentally measured up to 67 GHz. Nevertheless, the aforementioned lines, [27], [38], were realized using smooth and homogeneous copper sheets manually attached onto the substrate. Therefore, the measurements reported in this section represent the first experimental characterization of a printed textile microstrip line up to 50 GHz.

Observing the $S_{11,21}$ response in Fig. 15, it can be seen that the microstrip line maintains a matched ($S_{11} < -10$ dB) bandwidth from 1.98 GHz, with a -3 dB pass-band starting at 1.2 GHz. Observing the phase and magnitude response during bending and after 100 bending cycles (over a 5 mm radius), it can be seen that the measured S_{21} is highly stable. With no VNA time-averaging or trace smoothing applied, the measured traces, using the setup in Fig. 11, maintained a stability of ±0.01 dB up to 50 GHz, highlighting the reliability of the screen-printed textile lines.

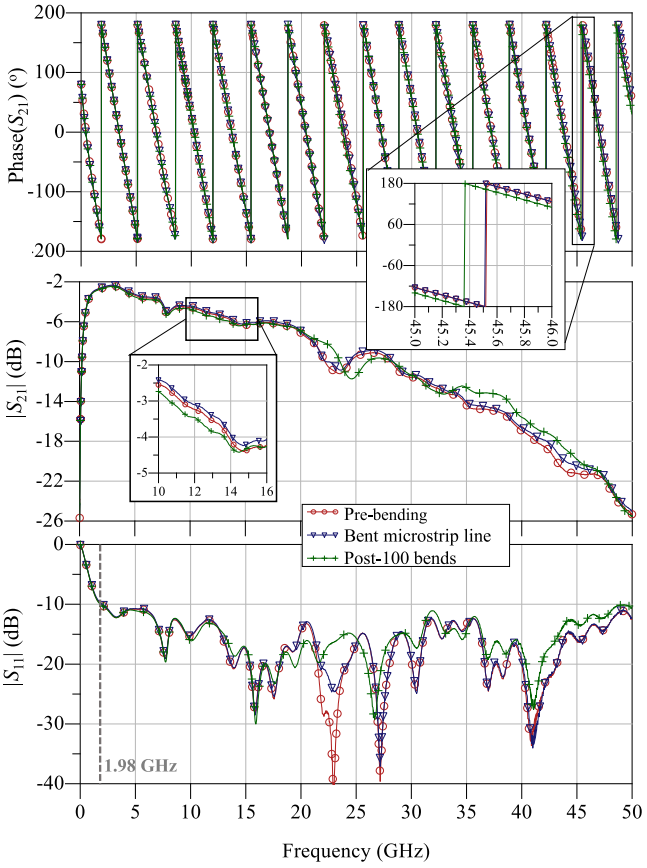

FIGURE 15. Measured s-parameters of the textile capacitor-impregnated microstrip line up to 50 GHz before, during, and after repeated bending.

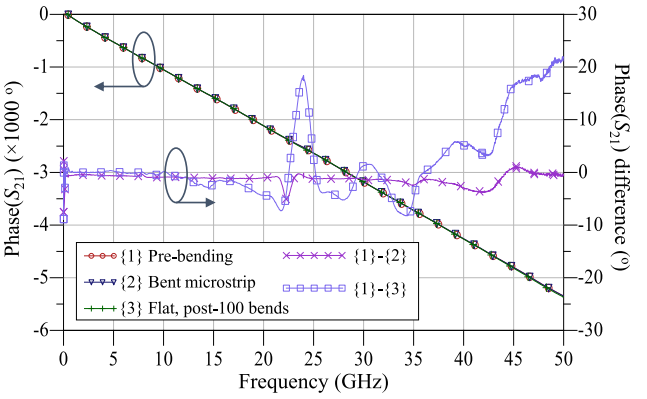

FIGURE 16. Measured unwrapped phase difference across the three measurements of the same microstrip line, before, during, and after 100 bends.

In terms of phase stability, the unwrapped phase response of the woven polyester-cotton line, from Fig 11(a), is shown in Fig. 16. On the secondary axis of Fig. 16, it can be seen that the phase difference between the pre-bending and post/during-bending measurements is under 20°, translating to under 0.8% phase variation, at 25GHz, and around 0.4% phase difference at 50 GHz. Moreover, a stable group delay,

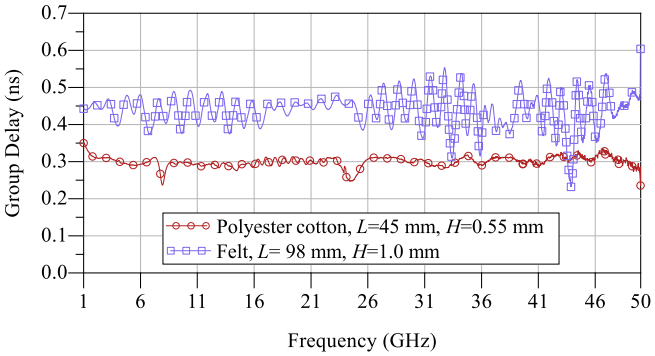

FIGURE 17. Measured group delay of the felt and polyester-cotton based microstrip lines across their matched S_{11} bandwidth.

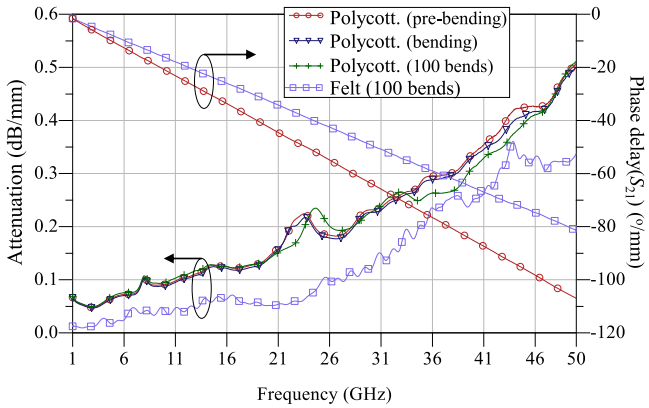

FIGURE 18. Measured attenuation and phase delay of the capacitor-impregnated mmWave lines across their matched ($S_{11} < -10$) bandwidth for both substrates investigated.

for both the felt-based and woven polyester-based lines, can be observed in Fig. 17.

The measured insertion losses and phase delay of both lines have been normalized to the lines' lengths and are shown in Fig. 18. It is evident that the felt-based line maintains lower attenuation, in dB/mm, compared to the thinner and lower tanδ woven-polyester counterpart. This is attributed to its wider trace resulting in a lower Ohmic resistance. Therefore, the felt-based microstrip line exhibits lower attenuation across its full bandwidth, despite being implemented on a thicker substrate with a higher tanδ. Therefore, it can be concluded that in transmission lines realized using relatively low conductivity inks, the primary design goal should be minimizing the Ohmic losses, as opposed to the dielectric losses, even when the line is implemented on relatively lossy (tan$\delta = 0.02$) substrates. The lower phase delay in the felt line is attributed to its lower permittivity ($\epsilon_r \approx 1.2$) whereas $\epsilon_r \approx 1.7$ for the polyester cotton substrate. For both lines, it can be concluded that screen-printed textile microstrip lines are suitable for mmWave applications such as compact antennas feedlines, with less than 1 dB/mm loss at 50 GHz.

The proposed screen-printed textile-based microstrip lines are compared in Table 1. Comparing the measured insertion

TABLE 1. Comparison With Other Printed and Flexible Transmission Lines

	This work	[18]	[22]	[23]
Transmission Line	Microstrip w/ capacitor	Contact-less CPW	Microstrip with 3D vias	CPW
DC Blocking	yes	yes	no	no
Meas. pass-band	(0.08–1.2)–50 GHz	0.1–5 GHz	DC–40 GHz	DC–110 GHz
Substrate	rough fabric: felt, polyester-cotton ($\tan\delta$ >0.01)	paper ($\tan\delta$ >0.01**)	LCP, glass, ABS	LCP, Kapton
Rough substrate	Yes	no	no	no
Fabrication	Screen-printing	Inkjet printing	Spray coating	Aerosol jetting
α (dB/mm)	0.02 dB/mm @ 1 GHz; 0.35 dB/mm @ 50 GHz	0.4 dB/mm at 1–5 GHz	0.14 dB/mm @ 1 GHz*; 0.53 dB/mm @ 40 GHz	0.3 dB/mm @ 50 GHz; 0.6 dB/mm @ 110 GHz*†

*Estimated from the graphs;
**based on previous paper $\tan\delta$ measurements [39];
† α for a Kapton substrate

losses to aerosol-jetted silver ink lines [22], it can be seen that despite being fabricated on lossier and rougher substrates, and containing an embedded DC-blocking capacitor of up to 44 pF capacitance, the realized screen-printed microstrip lines exhibits lower losses up to 50 GHz. In addition, compared to the only reported printed DC-blocking capacitively-coupled transmission line, [18], the proposed lines exhibit significantly improved insertion losses, as well as a very uniform phase and magnitude response over a 10× wider bandwidth. In addition, based on the simulated and measured response of the proposed line, it is anticipated that the operation bandwidth of the line is higher than 50 GHz. However, the measured s-parameters were restricted by the measurement setup. With a measured matched S_{11} response up to 50 GHz, a stable group-delay, and a very reproducible s-parameters response, the proposed multi-layered DC-blocking microstrip lines are highly suitable for mmWave applications.

V. CONCLUSION

In this paper, a novel microstrip-embedded parallel-plate capacitor was proposed based on screen-printing for flexible microwave and mmWave components. By integrating the capacitor's plates within an impedance-controlled microstrip line, low-cost low-resolution printed capacitors can operate as DC-blocks up to 50 GHz, without altering the mode-free propagation response of the line. The proposed capacitors were implemented on two textile substrates exhibiting minimal increase in the insertion losses. The capacitor-impregnated microstrip lines exhibit amatched S_{11} up to 50 GHz, with the closed-form calculations, 3D full-wave simulations, and experimental measurements in good agreement. The capacitor-impregnated microstrip line shows a repeatable uniform measured phase response with less than 0.8% phase variations, a stable group delay, as well as a stable S_{21} response under and during bending, as well as after 100 bends. Our comparisons between the analytical, numerical, and experimental insertion losses in the rough, low-conductivity, fabric-based microstrip highlight the need for more accurate modelling of conductor losses in textile-based and printed transmission lines with a relatively low conductivity.

Several novel contributions to printed microstrip passives have been presented in this work. First of all, the proposed microstrip-embedded capacitor represents over ten fold improvement in the operation frequency over reported printed RF capacitors. Secondly, the realization of screen-printed microwave and mmWave microstrip lines on rough substrates such as felt fabric represents a significant improvement in scalable manufacturing of microwave e-textile components. In addition, the experimental characterization of the insertion losses through the textile-based printed microstrip lines represents the highest frequency measurement of a textile-based printed transmission line reported to-date. Furthermore, the realized DC-blocking lines exhibit the widest bandwidth compared to all distributed elements DC-blocks reported in literature. Finally, compared to commercial lumped capacitors, it was demonstrated that the proposed microstrip-embedded capacitor exhibits higher mechanical reliability as well as better high-power handling capability.

ACKNOWLEDGMENT

The authors would like to thank Aran Amin for providing the SEM images, Terry Harvey for providing the surface profile measurement, Andrew Cruden for providing the Fluke thermal imager, and Harold Chong for providing the PNA E-calibration kit. Datasets used in this article are available from the University of Southampton repository at DOI: 10.5258/SOTON/D2024

REFERENCES

[1] S. A. Nauroze *et al.*, "Additively manufactured RF components and modules: Toward empowering the birth of cost-efficient dense and ubiquitous IoT implementations," *Proc. IEEE*, vol. 105, no. 4, pp. 702–722, Apr. 2017.
[2] R. Bahr, B. Tehrani, and M. M. Tentzeris, "Exploring 3-D printing for new applications: Novel inkjet- and 3-D-printed millimeter-wave components, interconnects, and systems," *IEEE Microw. Mag.*, vol. 19, no. 1, pp. 57–66, Jan./Feb. 2018.
[3] B. S. Cook, B. Tehrani, J. R. Cooper, and M. M. Tentzeris, "Multilayer inkjet printing of millimeter-wave proximity-fed patch arrays on flexible substrates," *IEEE Antennas Wireless Propag. Lett.*, vol. 12, pp. 1351–1354, Oct. 2013.
[4] M. Wagih, A. S. Weddell, and S. Beeby, "Meshed high-impedance matching network-free rectenna optimized for additive manufacturing," *IEEE Open J. Antennas Propag.*, vol. 1, pp. 615–626, 2020.
[5] A. Meredov, K. Klionovski, and A. Shamim, "Screen-printed, flexible, parasitic beam-switching millimeter-wave antenna array for wearable applications," *IEEE Open J. Antennas Propag.*, vol. 1, pp. 2–10, 2020.

[6] T.-H. Lin, S. N. Daskalakis, A. Georgiadis, and M. M. Tentzeris, "Achieving fully autonomous system-on-package designs: An embedded-on-package 5G energy harvester within 3D printed multilayer flexible packaging structures," in *Proc. IEEE MTT-S Int. Microw. Symp.*, 2019, pp. 1375–1378.

[7] B. S. Cook, J. R. Cooper, and M. M. Tentzeris, "Multi-layer RF capacitors on flexible substrates utilizing inkjet printed dielectric polymers," *IEEE Microw. Wireless Compon. Lett.*, vol. 23, no. 7, pp. 353–355, Jul. 2013.

[8] T. W. Whittaker, W. G. Whittow, and J. C. Vardaxoglou, "Artificially engineered capacitors for discrete high-frequency electronic circuitry," *IEEE Trans. Microw. Theory Techn.*, vol. 68, no. 1, pp. 74–86, Jan. 2020.

[9] M. Wagih, N. Hillier, S. Yong, A. S. Weddell, and S. Beeby, "RF-powered wearable energy harvesting and storage module based on E-textile coplanar waveguide rectenna and supercapacitor," *IEEE Open J. Antennas Propag.*, vol. 2, pp. 302–314, Feb. 2021.

[10] D. Kajfez and B. Vidula, "Design equations for symmetric microstrip DC blocks," *IEEE Trans. Microw. Theory Techn.*, vol. 28, no. 9, pp. 974–981, Sep. 1980.

[11] T. Koscica, "Microstrip quarter-wave high voltage DC block," *IEEE Trans. Microw. Theory Techn.*, vol. 41, no. 1, pp. 162–164, Jan. 1993.

[12] T. E. Koscica, "Wide-band ground-plane DC block and bias feed," *IEEE Trans. Microw. Theory Techn.*, vol. 38, no. 6, pp. 805–806, Jun. 1990.

[13] D. Lacombe and J. Cohen, "Octave-band microstrip DC blocks (Short Papers)," *IEEE Trans. Microw. Theory Techn.*, vol. 20, no. 8, pp. 555–556, Aug. 1972.

[14] H.-R. Ahn and T. Itoh, "Impedance-transforming symmetric and asymmetric DC blocks," *IEEE Trans. Microw. Theory Techn.*, vol. 58, no. 9, pp. 2463–2474, Sep. 2010.

[15] M. Umar, M. Laabs, N. Neumann, and D. Plettemeier, "Design of DC-blocks and bias-tee on PCB for V-band," *IEEE Microw. Wireless Compon. Lett.*, vol. 31, no. 10, pp. 1107–1110, Oct. 2021.

[16] S.-H. Choi, J.-Y. Lee, K.-B. Lee, and D.-H. Shin, "Design of miniaturized symmetric microstrip DC block," in *Proc. Asia-Pacific Microw. Conf.*, 2007, pp. 1–4.

[17] M. Liang, X. Yu, C. Shemelya, E. MacDonald, and H. Xin, "3D printed multilayer microstrip line structure with vertical transition toward integrated systems," in *Proc. IEEE MTT-S Int. Microw. Symp.*, 2015, pp. 1–4.

[18] L. Xie, Y. Feng, G. Yang, Q. Chen, and L.-R. Zheng, "RF interconnections for paper electronics," *IEEE Microw. Wireless Compon. Lett.*, vol. 25, no. 10, pp. 684–686, Oct. 2015.

[19] C. Mariotti, F. Alimenti, L. Roselli, and M. M. Tentzeris, "High-performance RF devices and components on flexible cellulose substrate by vertically integrated additive manufacturing technologies," *IEEE Trans. Microw. Theory Techn.*, vol. 65, no. 1, pp. 62–71, Jan. 2017.

[20] C. Mariotti, B. S. Cook, L. Roselli, and M. M. Tentzeris, "State-of-the-art inkjet-printed metal-insulator-metal (MIM) capacitors on silicon substrate," *IEEE Microw. Wireless Compon. Lett.*, vol. 25, no. 1, pp. 13–15, Jan. 2015.

[21] D. Vital, J. Zhong, S. Bhardwaj, and J. L. Volakis, "Loss-characterization and guidelines for embroidery of conductive textiles," in *Proc. IEEE Int. Symp. Antennas Propag. USNC/URSI Nat. Radio Sci. Meeting*, 2018, pp. 1301–1302.

[22] F. Cai, Y.-H. Chang, K. Wang, C. Zhang, B. Wang, and J. Papapolymerou, "Low-loss 3-D multilayer transmission lines and interconnects fabricated by additive manufacturing technologies," *IEEE Trans. Microw. Theory Techn.*, vol. 64, no. 10, pp. 3208–3216, Oct. 2016.

[23] M. Abt *et al.*, "Aerosol-printed highly conductive AG transmission lines for flexible electronic devices," *IEEE Trans. Compon. Packag. Manuf. Technol.*, vol. 8, no. 10, pp. 1838–1844, Oct. 2018.

[24] W. G. Whittow *et al.*, "Inkjet-printed microstrip patch antennas realized on textile for wearable applications," *IEEE Antennas Wireless Propag. Lett.*, vol. 13, pp. 71–74, Jan. 2014.

[25] I. Martinez *et al.*, "Compact, low-profile and robust textile antennas with improved bandwidth for easy garment integration," *IEEE Access*, vol. 8, pp. 77490–77500, 2020.

[26] M. Wagih, G. S. Hilton, A. S. Weddell, and S. Beeby, "Broadband millimetre-wave textile-based flexible rectenna for wearable energy harvesting," *IEEE Trans. Microw. Theory Techn.*, vol. 68, no. 11, pp. 4960–4972, Nov. 2020.

[27] N. Chahat, M. Zhadobov, S. A. Muhammad, L. L. Coq, and R. Sauleau, "60-GHz textile antenna array for body-centric communications," *IEEE Trans. Antennas Propag.*, vol. 61, no. 4, pp. 1816–1824, Apr. 2013.

[28] T. C. Baum, R. W. Ziolkowski, K. Ghorbani, and K. J. Nicholson, "Embroidered active microwave composite preimpregnated electronics-pregtronics," *IEEE Trans. Microw. Theory Techn.*, vol. 64, no. 10, pp. 3175–3186, Oct. 2016.

[29] Y. Li, R. Torah, S. Beeby, and J. Tudor, "An all-inkjet printed flexible capacitor on a textile using a new poly(4-vinylphenol) dielectric ink for wearable applications," in *Proc. IEEE SENSORS*, 2012, pp. 1–4.

[30] S.-E. Adami *et al.*, "A flexible 2.45-GHz power harvesting wristband with net system output from −24.3 dBm of RF power," *IEEE Trans. Microw. Theory Techn.*, vol. 66, no. 1, pp. 380–395, Jan. 2018.

[31] R. Del-Rio-Ruiz, J.-M. Lopez-Garde, J. Legarda, S. Lemey, O. Caytan, and H. Rogier, "Reliable lab-scale construction process for electromagnetically coupled textile microstrip patch antennas for the 2.45 GHz ISM band," *IEEE Antennas Wireless Propag. Lett.*, vol. 19, no. 1, pp. 153–157, Jan. 2020.

[32] M. Wagih, A. S. Weddell, and S. Beeby, "Omnidirectional dual-polarized low-profile textile rectenna with over 50% efficiency for sub-μW/cm^2 wearable power harvesting," *IEEE Trans. Antennas Propag.*, vol. 69, no. 5, pp. 2522–2536, May 2021.

[33] X. Chen, H. He, Z. Khan, L. Sydänheimo, L. Ukkonen, and J. Virkki, "Textile-based batteryless moisture sensor," *IEEE Antennas Wireless Propag. Lett.*, vol. 19, no. 1, pp. 198–202, Jan. 2020.

[34] M. Wagih, Y. Wei, A. Komolafe, R. Torah, and S. Beeby, "Reliable UHF long-range textile-integrated RFID tag based on a compact flexible antenna filament," *Sensors*, vol. 20, no. 12, 2020, Art. no. 3435.

[35] B. Smith, "Energy and power handling capabilities of thin film and ceramic capacitors," AVX Technical Information. Accessed: Sep. 22, 2021. [Online]. Available: https://www.avx.com/docs/techinfo/RFMicrowaveThinFilm/energytf.pdf

[36] G. Gold and K. Helmreich, "A physical model for skin effect in rough surfaces," in *Proc. 7th Eur. Microw. Integr. Circuit Conf.*, 2012, pp. 631–634.

[37] S. Hall *et al.*, "Multigigahertz causal transmission line modeling methodology using a 3-D hemispherical surface roughness approach," *IEEE Trans. Microw. Theory Techn.*, vol. 55, no. 12, pp. 2614–2624, Dec. 2007.

[38] M. Wagih, A. S. Weddell, and S. Beeby, "Millimeter-wave textile antenna for on-body RF energy harvesting in future 5G networks," in *Proc. IEEE Wireless Power Transfer Conf.*, 2019, pp. 245–248.

[39] V. Palazzi *et al.*, "A novel ultra-lightweight multiband rectenna on paper for RF energy harvesting in the next generation LTE bands," *IEEE Trans. Microw. Theory Techn.*, vol. 66 no. 1, pp. 366–379, Jan. 2018.

MAHMOUD WAGIH (Member, IEEE) received the B.Eng. degree (hons.) and the Ph.D. degree on rectenna design both in electrical and electronic engineering from the University of Southampton, Southampton, U.K., in 2018 and 2021, respectively.

In 2017, he worked as a Research Assistant with the University of Southampton, Malaysia. In 2018, he was a Hardware Engineering Intern with Arm, and, in 2020, a Research Intern with Arm, Cambridge, U.K. He currently holds the U.K. Royal Academy of Engineering UK IC Research Fellowship with the University of Southampton, Southampton, U.K. He has more than 50 refereed journal and conference publications, and has delivered several invited webinars on these topics. His research interests broadly cover antennas and microwave systems in energy harvesting, sensing, and wearable applications.

Dr. Wagih is a Senior Member of the International Union of Radio Science (URSI) and a member of the Institute of Engineering and Technology (MIET). He is an affiliate member of the IEEE Microwave Theory & Techniques Technical Committees TC-24 and TC-26. He was the recipient of the Best Undergraduate Project Prize, School Winner Doctoral Research Award, Best in Faculty Doctoral Research Award, and the Dean's Award for Early Career Researchers, during 2018–2021, at the University of Southampton. He was selected for the IEEE International Microwave Symposium Project Connect in 2019. He was the recipient of the Best Student Paper Award at the IEEE Wireless Power Transfer Conference, 2019, the Best Oral Paper at PowerMEMS, 2019, was a Best Student Paper Finalist at IEEE WPTC, 2021, and received the IEEE MTT-S Best 3MT Presentation Prize (second place) at the IEEE Microwave Week, 2020. He was the session Co-Chair at EuCAP, 2021, and a TPC reviewer for IEEE APS 2021 and IEEE FLEPS 2021. He acts as a reviewer for more than ten Transactions and journals.

ABIODUN KOMOLAFE (Member, IEEE) received the B.Sc. degree (Hons.) in physics from the University of Ibadan, Ibadan, Nigeria, in 2007, the M.Sc. degree in microelectromechanical systems, in 2011, and the Ph.D. degree in printed circuits on fabrics from the University of Southampton, Southampton, U.K., in 2016.

He currently works as a Research Fellow with the University of Southampton in investigating novel manufacturing methods for making functional electronics on textiles using flexible electronic circuits and screen-printed electronics for medical applications. He is experienced in the design and fabrication of e-textiles using screen printing and thin-film technologies.

NICHOLAS HILLIER received the Master of Physics (M.Phys.) degree from the University of Southampton, Southampton, U.K., in 2013 before joining the National Physical Laboratory (NPL). He is a Chartered Physicist currently undertaking the Ph.D. degree as part of the Energy Storage and its Applications CDT with the University of Southampton, Southampton, U.K. Since leaving NPL in 2017, his research interests has been include the power management of e-textiles, specifically looking to integrate supercapacitors and batteries directly into textiles.